



Structural, Magnetic and Microwave Absorption Properties of $\text{Ba}_{0.5}\text{Sr}_{0.5}\text{Ni}_{2-x}(\text{MgZn})_{x/2}\text{Fe}_{16}\text{O}_{27}$ Hexaferrite Nanoparticles Prepared by the Sol-Gel Combustion Method

Gholamreza Amiri¹

Received: 26 February 2018 / Accepted: 25 April 2018 / Published online: 29 June 2018
© Springer Science+Business Media, LLC, part of Springer Nature 2018

Abstract

In this study, Sr–Ba hexaferrite nanoparticles ($\text{Ba}_{0.5}\text{Sr}_{0.5}\text{Ni}_{2-x}(\text{MgZn})_{x/2}\text{Fe}_{16}\text{O}_{27}$, $x = -0.6$, in the step of 0.2) was synthesized by the sol-gel method. The influence of Mg–Zn substitution on the structure and microwave absorption properties of Ni–W-type hexaferrite were investigated by technical methods such as x-ray diffraction, vector network analyzer, transmission electron micrograph and vibrating sample magnetometer. TEM images illustrated almost spherical particles with an average size of 35–52 nm. The M–H loops for all samples were measured at room temperature by vibrating sample magnetometer. Saturation magnetization (M_s) and coercivity (H_c) were derived from the hysteresis loops. The maximum field used in this measurement was 9 kilo-Oersted (kOe). Finally, the microwave absorption properties of these samples were investigated in Ku band range. The thickness of the composites was 2 mm in microwave absorption measurements. The results showed that the synthesized samples have a great potential in many fields of industry.

Keywords Ferrite · Magnetic material · Nanoparticle · Absorption properties

1 Introduction

Electromagnetic absorbers are a critical part of defense systems due to their contribution to survivability in air vehicles. They are also used as commercial products in electromagnetic interference shielding [1–4]. The nanomaterial technology opened the door for new opportunities to further improve the functionality of electromagnetic absorbers. The use of nanoparticles in polymeric systems has become the subject of interest in engineering applications due to dramatic optional changes in composites physical properties [5, 6]. These changes are created due to increased surface area, which can increase the quantum effect of the materials [7]. These factors can change or enhance many properties of composites such as reactivity, strength, dielectric, and electromagnetic properties [8, 9].

A nanocomposite is a matrix that is produced by adding nanoparticles in order to improve a particular property of the material. The properties of nanocomposites have caused the researchers to use them in several fields. One

of the most important applications of nanocomposite is in the field of microwave absorber and many recent studies have focused on magnetic nanocomposites as a microwave absorber [10, 11]. One of the most applicable nanomagnetic materials used in microwave absorption is hexagonal ferrite. Hexagonal ferrites are suitable materials for radar-absorbing material due to their high permeability, high magnetization, planar anisotropic behavior, and good dielectric properties at microwave frequencies. In general, hexagonal ferrites are divided into six types: M, X, U, Y, Z, and W [12].

Many papers have been written about microwave-absorbing materials based on M-type hexagonal ferrites [13–16]. In the last decade, special attention has been paid to the use of the W-type ferrite in the design of radar-absorbing materials [17–20].

The crystal structure in the W-type ferrite is in the form of $\text{RSSR}^*\text{S}^*\text{S}$. In this structure, S is one-block spinel with two oxygen-ion layer block with composition of Fe_6O_8 and R is a three oxygen-ion layer block with composition of $\text{Ba}(\text{Or Sr})\text{Fe}_6\text{O}_{11}$. The asterisk sign (*) represents the 180° rotation of the block along the hexagonal axis [21].

Many researchers have shown that the replacement of divalent, trivalent, and tetravalent cations in hexagonal ferrite structure has a significant effect on the qualitative

✉ Gholamreza Amiri
amiri@iaufala.ac.ir

¹ Falavarjan Branch, Islamic Azad University, Isfahan, Iran

improvement of magnetism properties, especially microwave absorption.

Hitherto, many studies have been carried out on $\text{BaMe}_2\text{Fe}_{16}\text{O}_{27}$ and $\text{SrMe}_2\text{Fe}_{16}\text{O}_{27}$ [17–20]. But less attention has been paid to the W-type ferrite based on the common strontium and barium ($\text{Ba}_{0.5}\text{Sr}_{0.5}\text{Me}_2\text{Fe}_{16}\text{O}_{27}$) [22]. According to this approach, nanoparticles of the composition $\text{Ba}_{0.5}\text{Sr}_{0.5}\text{Ni}_{2-x}(\text{MgZn})_{\frac{x}{2}}\text{Fe}_{16}\text{O}_{27}$ were prepared by the sol-gel method and investigated the magnetic and microwave absorption properties.

2 Experimental Procedures

W-type strontium-barium hexaferrite powders were prepared by the citrate sol-gel method using ferric nitrate, barium nitrate, strontium nitrate, zinc nitrate, magnesium nitrate, nickel nitrate, ammonia, and citric acid as raw materials. In the first step, stoichiometric amounts of ferric nitrate, barium nitrate, strontium nitrate, zinc nitrate, magnesium nitrate, and nickel nitrate were dissolved together in a minimum amount of citric acid aqueous solution at 80 °C according to the formula: $\text{Ba}_{0.5}\text{Sr}_{0.5}\text{Ni}_{2-x}(\text{MgZn})_{\frac{x}{2}}\text{Fe}_{16}\text{O}_{27}$ ($x = 0-0.6$, in the step of 0.2). The molar ratios of citric acid to metal ions used were 1:1. Then, ammonia solution drop by drop was added until the solution attained pH 7. Afterwards, the solution was gradually warmed and a homogeneous gel was obtained. In the next step, the remaining materials were dried instantly in an oven at the temperature range of 120–140 °C. At the end of this process, the dried gel was calcined at 1200 °C for 2 h.

Microwave absorption properties were studied using standing wave ratio (SWR) method. The details of the measurement process are explained in our previous work [16]. The thickness of the composites in this study was 2 mm. X-ray diffractometer (XRD) with $\text{Cu-K}\alpha$ radiation was used to study the phase structure.

The size, particle shape, and microstructure were detected by transmission electron microscopy (TEM) JEOL1230 with an accelerating voltage of 200 kV. The magnetic properties of the powder samples were monitored at room temperature with a vibrating sample magnetometer (VSM).

3 Results and Discussions

3.1 Crystal structure

XRD patterns of the samples (calcined powders at 1200 °C) are shown in Fig. 1. In all XRD patterns, the main phase was observed the M-type hexaferrite phase and no additional phase were observed in these patterns. Lattice parameters are calculated for samples using the XRD results [23, 24]

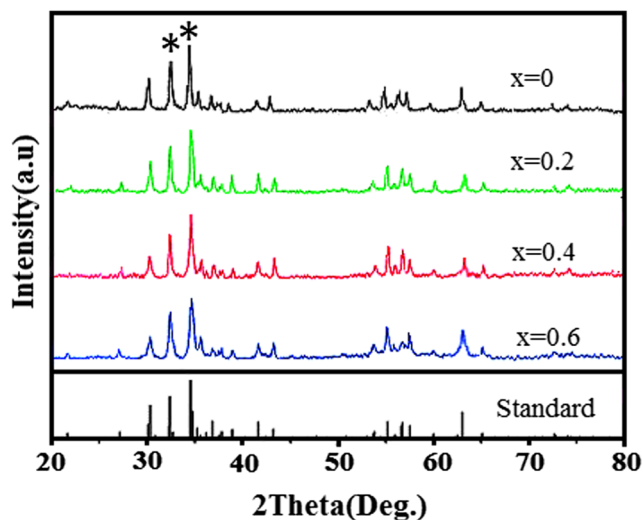


Fig. 1 XRD pattern of calcined powders at 1200 °C

and the calculated values are listed in Table 1. From Table 1, it can be seen that with increasing dopant ions, lattice constants are changed. These variations are due to the differences in ion radius (Ni ions are replaced with Mg and Zn).

The cell volume of the samples was obtained using the relation $V_C = 0.866a^2c$ [25]. The findings indicate that cell volume decreases with increasing Mg–Zn concentration. According to these results, it can be deduced that the samples have been somewhat contracted.

The size of the crystals was calculated using the Scherrer formula (42–56 nm) [26, 27]. Intense peaks 4 and 5 were used to calculate the average crystalline size. The peaks 4 and 5 are shown in Fig. 1 with the asterisk sign. TEM images for all samples are shown in Fig. 2. The images show that the particle size in this study is in the nanometer range ($D < 100$ nm). Using these images, the average particle size is between 36 and 56 nm.

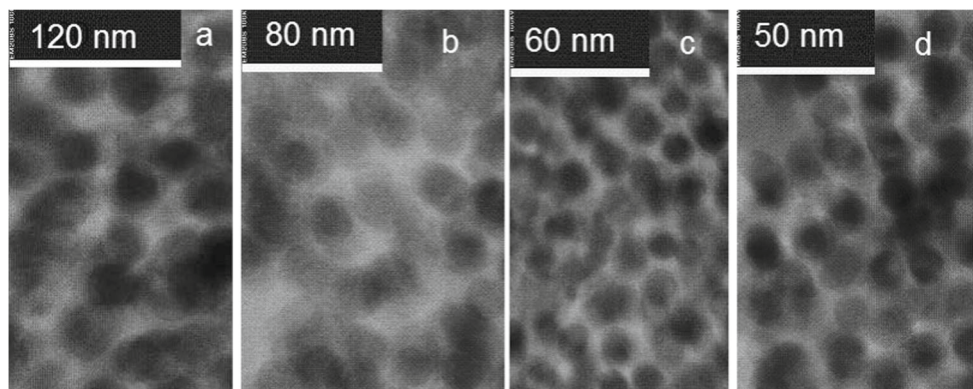
3.2 Magnetic Properties

Figure 3 shows the M–H loops for the synthesized samples. Saturation magnetization (M_s) and coercive force (H_c) were obtained using M–H loops and the values are listed in Table 1. From Fig. 3, it is clear that by increasing Mg–Zn concentration, saturation magnetization is decreased.

Table 1 The structural and magnetic parameters of $\text{Ba}_{0.5}\text{Sr}_{0.5}\text{Ni}_{2-x}(\text{MgZn})_{\frac{x}{2}}\text{Fe}_{16}\text{O}_{27}$

x	a (nm)	c (nm)	c/a	V (nm) ³	D (nm)	M_s	H_c
0	0.5802	3.324	5.729	0.9690	56	71	1100
0.2	0.5849	3.330	5.693	0.9865	53	67	1210
0.4	0.5867	3.340	5.692	0.9956	47	61	1320
0.6	0.5890	3.321	5.638	0.9977	42	58	1520

Fig. 2 TEM micrographs of prepared powders. **a** $x = 0$. **b** $x = 0.2$. **c** $x = 0.4$. **d** $x = 0.6$



The decrease in saturation magnetization is due to the spin canting [28]. Replacing nickel cations with magnesium cations creates vacancies in the structure. These vacancies cause the spins to cant, and as a result, the distribution of cations changes. The magnetic moments of Ni, Zn, and Mg ions are 2, 0, and 0 μB , respectively. Given these magnetic moments, these ions are not able to cancel out with spin-down moments of Fe^{+3} ions (5 μB).

As can be seen from the values of Table 1, H_c increases with increasing the Mg–Zn concentration. Using the obtained results, it can be concluded that by increasing the Mg and Zn concentration, the samples are closed to the hard ferrites. It is a noteworthy and generally accepted fact that, the H_c depends on various parameters such as anisotropy, particle size, and saturation magnetization [29–32].

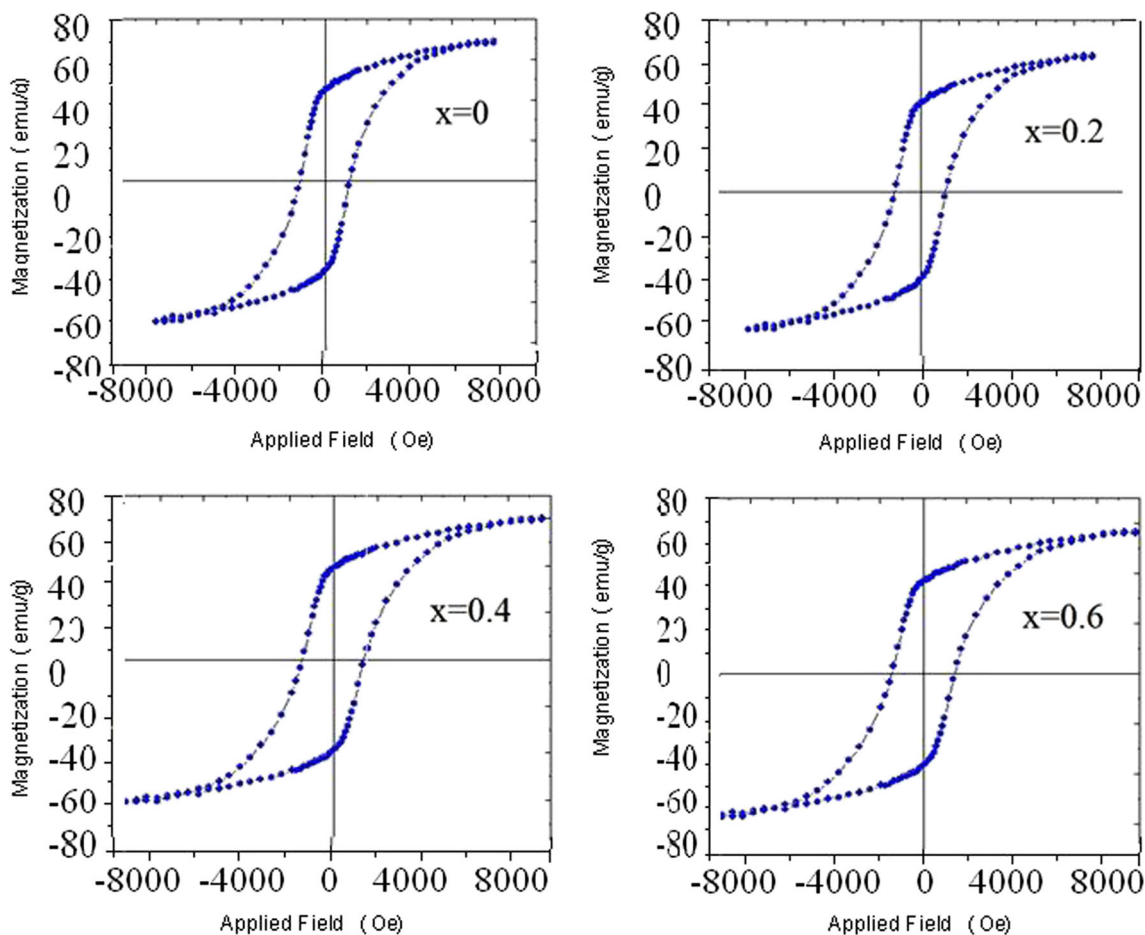


Fig. 3 Room-temperature hysteresis loops of $x = 0$, $x = 0.2$, $x = 0.4$, and $x = 0.6$

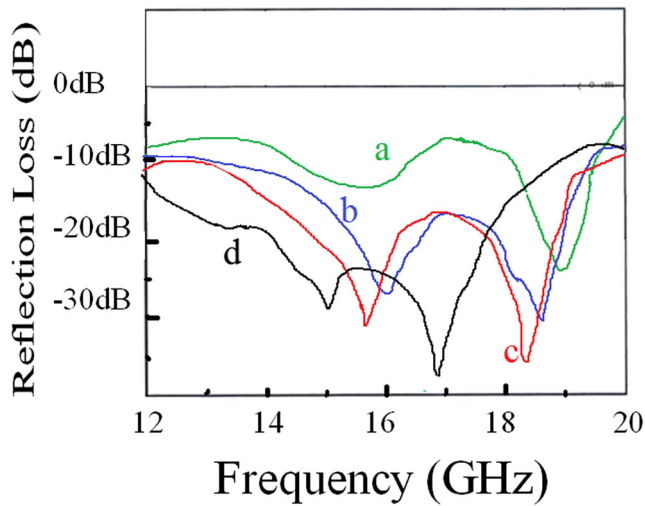


Fig. 4 Absorption characteristics of the composite. **a** $x = 0$. **b** $x = 0.2$. **c** $x = 0.4$. **d** $x = 0.6$

3.3 Attenuation Properties

Reflection losses are calculated from the theory of transmission lines. When an electromagnetic wave is brought to a ferrite surface on the back of which is a metallic surface, two processes of transition to ferrite and a reflection of the ferrite surface occur. The waves transmitted to the ferrite are reflected after it has reached the metal. This reflected wave after propagation in matter reaches again the ferrite surface. When the reflection waves from the surface of the metal and ferrite with each other have a phase difference of 180° , they will eliminate each other and the result of the reflective wave will be zero. This condition occurs when the ferrite thickness is one fourth of the wavelength or odd integer multiple of the wavelength.

The reflection loss (RL) could be described as [33]:

$$RL(\text{dB}) = 20 \log \left| \frac{Z_{in} - Z_0}{Z_{in} + Z_0} \right| \tag{1}$$

In this formula, Z_0 is the intrinsic impedance of free space and Z_{in} is the composites impedance and is defined as follows [34]:

$$Z_{in} = \sqrt{\frac{\mu_r}{\epsilon_r}} \tanh \left[j \frac{2\pi}{c} \sqrt{\mu_r \epsilon_r} f d \right] \tag{2}$$

Table 2 Electromagnetic wave absorption properties of composites with 70 wt% ferrites

Composition (x)	Minimum RL value (dB)	Thickness (mm)	f (GHz) (minimum RL)	Frequency range (GHz) (RL < -15 dB)
$x = 0$	-24	2	18.9	1.1
$x = 0.2$	-30	2	18.6	4.4
$x = 0.4$	-36	2	18.2	4.1
$x = 0.6$	-37.66	2	16.9	5.7

wherein c , d , f , μ_r , and ϵ_r are the light velocity, thickness of composite, frequency of the incident EM wave, complex permeability, and complex permittivity, respectively. The impedance matching condition is given by $Z_{in} = 1$, to represent the perfect absorbing properties.

A required absorbent and operational feature has four characteristics: low thickness, low mass, wide range of frequency, and high absorbency (weak reflection). Operationally, however, it is not straightforward to provide all of these four characteristics at the same time.

It is noted, for polycrystalline ferrites under an alternating current electromagnetic field, there are two various resonance mechanisms: the domain wall resonance and the resonance natural. Various experiments on spinel ferrites have shown that the natural resonance frequency is greater than the domain wall resonance. The resonant frequency is also a function of the anisotropy that can be defined from the following equation [35]:

$$f_R = \frac{1}{2\pi} \eta (H_\theta H_\phi)^{1/2} \tag{3}$$

In this formula η is the gyromagnetic ratio and H_θ H_ϕ are the out-of-plane and in-plane anisotropy fields, respectively. Equation (3) shows that the increase in magnetocrystalline anisotropy fields (H_θ and H_ϕ) results increases the resonant frequency.

Figure 4 illustrate the RL curves of synthesized samples with 2-mm thickness and 70 wt% ferrites in Ku band range. It is noted that in the present study, the bandwidth is determined as the frequency width in which the reflectance is less than -15 dB. In Table 2, the results of the absorption properties for composites are listed.

According to Fig. 4 the undoped W-type ferrite has a minimum reflection loss of -24 dB at 18.9 GHz (Fig. 4a). Figure 4b is shown the minimum RL of -30 and -27.4 dB for composition with “ $x = 0.2$ ” at 18.4 and 16 GHz frequencies, respectively, with a bandwidth of 4.4 GHz, covering a frequency range from 14.8 to 19.2 GHz.

For sample “ $x = 0.4$ ” Fig. 4c showed two minimum reflection loss at of 16 and 18.6 GHz frequencies. In the samples studied in this study, the minimum reflection loss value increases from -24.00 dB in the composition with $x = 0$ to -37.66 dB in the composition with $x = 0.6$ at 16.9 GHz. From the results, it can be seen that

with increased magnesium/zinc concentration, the loss of absorption increases.

4 Conclusions

With regard to the results, it is inferred that the sol-gel method is suitable for the preparation of W-type ferrites ($\text{Ba}_{0.5}\text{Sr}_{0.5}\text{Ni}_{2-x}(\text{MgZn})_{\frac{x}{2}}\text{Fe}_{16}\text{O}_{27}$). The characteristic specifications of hysteresis loops demonstrate the ferromagnetic nature of $\text{Ba}_{0.5}\text{Sr}_{0.5}\text{Ni}_{2-x}(\text{MgZn})_{\frac{x}{2}}\text{Fe}_{16}\text{O}_{27}$ hexaferrite at room temperature. It is also concluded from the results that the replacement of magnesium and zinc cations cause Ni–W-type ferrite to become hard type ferrite. From the results obtained, it can be deduced that the ferrites inferred in this research are promising candidates for industry applications such as camouflage and stealth technology in the future.

Acknowledgments The authors are grateful to Falavarjan Branch, Islamic Azad University, for their cooperation in this work.

References

1. Sharbati, A. et al.: Solid State Commun. **150**, 2218 (2010)
2. Bach, T.N. et al.: J. Alloys Compd. **695**, 1658 (2017)
3. Verma, M. et al.: Phys. Chem. Chem. Phys. **17**, 1530 (2015)
4. Salman, S. et al.: Mater. Des. **112**, 462 (2016)
5. Tyagi, S. et al.: J. Alloys Compd. **731**, 584 (2017)
6. Juhua, L. et al.: J. Nanosci. Nanotechnol. **16**, 6049 (2016)
7. Kelly, K.L. et al.: J. Phys. Chem. B. **668**, 107 (2003)
8. Jinhao, G. et al.: Acc. Chem. Res. **42**, 1097 (2009)
9. Jackson, J.B. et al.: J. Phys. Chem. B **105**, 2743 (2001)
10. Wang, H.C. et al.: Rare Metals. **34**, 223 (2015)
11. Syazwan, M.M. et al.: J. Mater. Sci. Mater. Electron. **28**, 8429 (2017)
12. Sharbati, A. et al.: J. Nanomater. Biostruct. **1**, 187 (2011)
13. Dong, C. et al.: JMMM. **354**, 340 (2014)
14. Kaur, R. et al.: Solid State Commun. **201**, 72 (2015)
15. Narang, S.B. et al.: JMMM. **405**, 17 (2016)
16. Sharbati, A. et al.: Solid State Commun. **152**, 199 (2012)
17. Sharbati, A. et al.: Bull. Mater. Sci. **38**, 1 (2015)
18. Deng, L. et al.: JMMM **323**, 1895 (2011)
19. Shen, G. et al.: JMMM **301**, 325 (2006)
20. Yang, Y. et al.: JMMM **265**, 119 (2003)
21. Aen, F. et al.: Ceram. Int. **42**, 16077 (2016)
22. Ali, A. et al.: J. Electron. Mater. **46**, 903 (2017)
23. Lakshmi, M. et al.: J. Nanostruct. Chem. **5**, 365 (2015)
24. Aravind, G. et al.: J. Nanostruct. Chem. **5**, 77 (2015)
25. Ali, I. et al.: Mater. Res. Bull. **49**, 338 (2014)
26. Abedini Khorrami, S. et al.: Int. J. Nano Dimension **3**, 191 (2013)
27. Kumar, L. et al.: Int. Nano Lett. **3**, 1 (2013)
28. Akhtar, M.N. et al.: Int. J. Modern Phys. B. **25**, 2249 (2011)
29. Allaedini, G. et al.: Int. Nano Lett. **5**, 183 (2015)
30. Alamolhoda, S. et al.: Int. J. Nanosci. Nanotechnol. **13**, 195 (2017)
31. Rashidi, S. et al.: J. Ultrafine Grained Nanostruct. Mater. **48**, 59 (2015)
32. Nabyouni, G. et al.: J. Nanostruct. **7**, 77 (2017)
33. Mehdizadeh, P. et al.: J. Nanostruct. **6**, 140 (2016)
34. Azizi, F. et al.: J. Nanostruct. **5**, 345 (2015)
35. Sharbati, A. et al.: J. Mater. Sci. **24**, 3629 (2013)